Available online at www.sciencedirect.com

ScienceDirect

Procedia Engineering 67 (2013) 270 – 278

Procedia Engineering

www.elsevier.com/locate/procedia

7th Asian-Pacific Conference on Aerospace Technology and Science, 7th APCATS 2013

Effects of AC Dielectric Barrier Discharge plasma actuator location on flow separation and airfoil performance

Y. Bouremel[a,*], J. M. Li[a], Z. Zhao[b], M. Debiasi[a]

[a]Temasek Laboratories, National University of Singapore, Singapore 117411
[b]Department of Mechanical Engineering, National University of Singapore, Singapore 117411

Abstract

The goal of this work is to characterize the effect of Dielectric Barrier Discharge (DBD) plasma actuator on the lift and drag coefficients generated by the flow around a NACA 4415 airfoil model using force-balance and Particle Image Velocimetry (PIV) measurements. DBD actuators are mounted at the leading edge, at 30% and 60% of the chord length. The effect of actuation on the airfoil lift and drag at these different locations are studied. It is found that for increasing angles of attack, the actuators need to be located closer to the leading edge and in front of the separation area to produce the best lift or drag coefficient improvements. If located within the flow separation zone, their effects on the airfoil lift and drag coefficients are limited.

© 2013 The Authors. Published by Elsevier Ltd. Open access under CC BY-NC-ND license.
Selection and peer-review under responsibility of the National Chiao Tung University

Keywords: Dielectric Barrier Discharge Plasma; Particle Image Velocimetry; Vorticity; Lift Coefficient; Drag coefficient; Separation Point

Nomenclature

b	model span (from wall to wall of the wind tunnel) (m)
c	model chord (m)
C_D	drag coefficient (-)
C_L	lift coefficient (-)
Re	Reynolds number (-)
s	curvilinear coordinate (m)
x	streamwise coordinate of the wind tunnel (m)
y	spanwise coordinate of the wind tunnel (m)

* Corresponding author. Tel.: +65-6516-4789; fax: +65-6872-6840.
E-mail address: tslyb@nus.edu.sg

1877-7058 © 2013 The Authors. Published by Elsevier Ltd. Open access under CC BY-NC-ND license.
Selection and peer-review under responsibility of the National Chiao Tung University
doi:10.1016/j.proeng.2013.12.026

z	vertical coordinate of the wind tunnel (m)
Greek symbols	
α	angle of attack of the airfoil (deg)
ω	vorticity (s^{-1})
Subscripts	
act	coordinate of the actuator (m)
separation	coordinate of the separation point (m)

1. Introduction

Several studies demonstrate the ability of plasma actuators in active flow control. A review of Moreau [1] describes the topic of airflow control by non-thermal plasma actuators. This paper shows the recent knowledge concerning the electric wind induced by plasma actuators in quiescent air at atmospheric pressure. It also presents some active flow control applications by plasma actuators, and the effective results obtained for low-velocity airflows. In the work by Jolibois et al. [2], a study of airflow separation control above a NACA0015 airfoil by using seven DBD plasma actuators is presented. In this study, the velocity is 6 m/s, corresponding to Re = 0.4 x 10^6 based on a chord length of 1 m and the plasma actuators are placed on the upper surface from x/c = 0.3 to 0.78. The results show that this type of action is able to reattach a naturally detached airflow or to detach a naturally attached airflow. Control of flow separation over a flap of a high-lift airfoil using a single DBD plasma actuator has also been investigated [3]. The actuator is found to be most effective for increasing lift when operated in an unsteady fashion at the natural oscillation frequency of the trailing edge flow field. According to Little et al. [3], the possible mechanism is that free stream momentum is entrained into the separated region because of natural instabilities being amplified by the actuator hence reducing the size of the time averaged separation. Plasma actuators can also be mounted at the trailing edge of the airfoil to alter the overall circulation around the airfoil thanks to Coanda effect [4]. The current novel study is motivated to look into the relation between the position of the actuator on the airfoil relatively to the flow separation point and its effect on the drag and lift by combining flow visualization and force balance measurements.

2. Experimental set-up

Three DBD plasma actuators are mounted on a NACA 4415 airfoil model respectively at the leading edge, at 30% and at 60% of the chord length. The airfoil model is made of Plexiglas with a chord c of 100 mm and a span b of 158 mm. The actuators are made of 0.066 mm thick copper; the exposed electrode located at the leading edge is a baseline electrode while the two located downstream have a comb-like exposed electrode configuration. The dielectric between the exposed electrode and the buried electrode are made of PCB support of 1 mm thickness and two layers of Kapton sheet of 125 μm and 76.2 μm. Each actuator is independently driven to look at the relation between its position and the lift generated when it is turned on. The peak-to-peak voltage applied to the electrodes is 15.5 kV at a frequency of 5 kHz. The experiments are conducted at Re = 35000 based on the chord length of 0.1 m and a velocity of 5 m/s. The model is mounted on a turntable incorporating a balance. The model angle of attack α varies from -6° to 16°. The balance used to record the data is an ATI Mini40 piezoelectric gauge. Two axes are aligned with the streamwise and the vertical directions of the wind tunnel to measure the drag and the lift forces generated by the model. The recording sequence consists of 2 seconds with no actuation to define the baseline flow followed by 4 seconds with actuation. The sampling frequency is 1 kHz and the signal is low-pass filtered at 10 Hz before average in order to remove the effects of small vibrations induced by the flow. Flow-field velocity measurements are obtained by using a two-velocity-component Particle Image Velocimetry (PIV) system. The flow is uniformly seeded upstream of the wind-tunnel air intake with olive oil particles from a Dantec 10F03 seeding generator. Droplets are produced in the average size Sauter mean diameter (SMD) 2-5 μm whose reflections correspond to no more than 3 pixels in the captured images, which allow a good resolution of the

particle displacement when cross-correlation methods are adopted. A dual-head Litron DualPower 200-15 Nd:YAG laser operating at the second harmonic (532 nm) at approximately 150 mJ per pulse is used in conjunction with sheet-forming optics to form a thin sheet (~1 mm) on the *x-z* plane passing through the centerline of the test section. The images are acquired using double frame mode by a 2048 x 2048 pixels HiSense 620 camera with a Zeiss 50 mm f/2.0 macro lens (178.3 x 178.3 mm field of view). The resulting resolution is approximately 87 μm per pixel. The camera views the streamwise laser sheet orthogonally over the entire field of view. To retain a good resolution of the flow particles close to the upper surface of the model, a 527 to 537 nm band-pass optical filter is placed in front of the lens whereas the surface of the model exposed to the laser sheet is sprayed with clear acrylic paint containing rhodamine 6G (which fluoresces close to 566 nm when excited by 532 nm light). A computer with dual Intel Core processors is used for data acquisition. The acquired frames are divided into 32 x 32 pixel interrogation windows, which contain at least 3 seeding particles each. Based on the flow velocity and the size of the interrogation area, the time separation between the two laser flashes (double frame mode) is set such that the maximum displacement of a particle is no more than 25% of the interrogation size which is the optimum displacement for the Dantec software to calculate accurately the particle velocity. For each frame, subregions are adaptatively cross-correlated using multi-pass processing with a final 50% overlap that gives a final interrogation area of 16 x 16 pixels after processing. The resulting vector fields are post-processed to remove remaining spurious vectors. This arrangement gives a velocity vector grid of 127 x 127 points, which translates to velocity vectors separated by about 1.39 mm over the field of view. For each acquisition, 200 velocity-vector images are taken for averaging at a trigger rate of 7 Hz for the baseline flow and the experiments with the actuator switched on are repeated 4 times for statistical average.

3. Results and Discussions

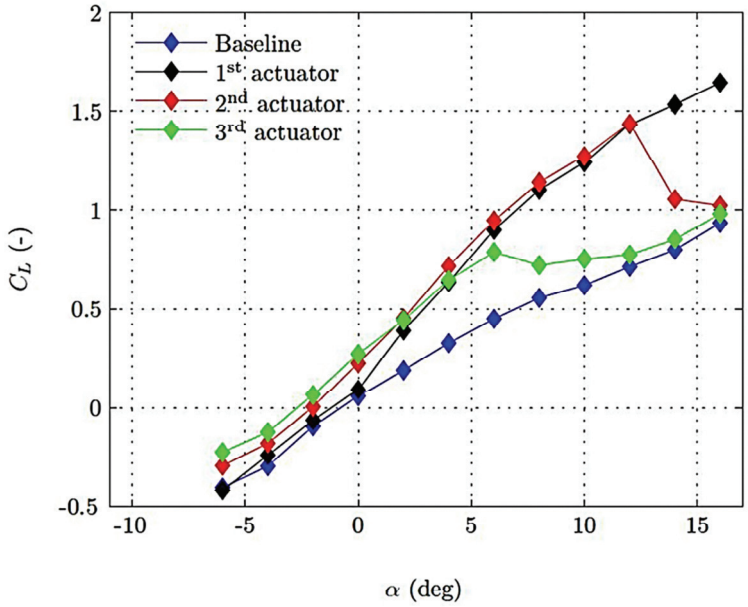
3.1. Force balance measurements

Force measurements are used to characterize the lift and drag coefficients when the actuators located along the airfoil are switched on one by one. The goal is to find which DBD plasma actuator produces the best lift and drag coefficients for a given angle of attack and to check whether there is a correlation between the position of the actuator and the angle of attack. Figures 1 (a)-(b) show the variations of the lift coefficient C_L and the drag coefficient C_D with α when the 1st, 2nd and 3rd actuators are switched on for Re = 35000. The 1st actuator is the leading edge one (black line) while the 2nd (red line) and the 3rd actuator (green line) are located at 30% and 60% of the chord length. The blue lines in Figs. 1 (a)-(b) represent the baseline conditions when no actuators are switched on. It can be seen in Fig. 1 (a) that for α ranging from -6° to 16°, the different actuators globally increase the C_L of the airfoil model with a maximum improvement by the 3rd actuator of nearly 4 times the baseline value C_L = 0.0570 obtained at α = 0°. It can be seen that the 3rd actuator (green line) generates a higher lift coefficient compared to the other actuators at negative angles up to 0°, while the 2nd actuator (red line) produces the largest C_L for angles between 2° and 10°. At high angles of attack between 12° and 16°, the plasma generated from the 1st actuator (black line) produces the largest lift coefficient. For example at -6°, the 3rd actuator generates the highest lift coefficient with a value slightly more than 44 % the baseline value, while at 16°, the first actuator generates the best lift coefficient with an improvement of 75.7 % over the baseline value. Therefore, the position of the actuator associated with the best C_L gets closer to the leading edge with increasing values of α. Concerning the drag coefficient shown in Fig. 1 (b), the plasma generated by the 3rd actuator generates the lowest drag up to 4°, which is a slightly larger α range compared to that for which the same actuator generates the best lift in Fig. 1 (a). Up to 12°, the airfoil has very similar drag coefficient when the plasma from the 2nd or the 1st actuator is switched on, for example C_D = 0.138 and 0.139 at 12° for the 1st and 2nd actuators, respectively. Above 12°, the drag is lower when the 1st actuator is turned on. The trend of the lift and drag generated by the 1st, 2nd and 3rd actuators are similar with approximately the same actuators generating the best lift or drag coefficients for the same range of angles of attack even if for some angles, the actuator producing the best lift may not be necessarily

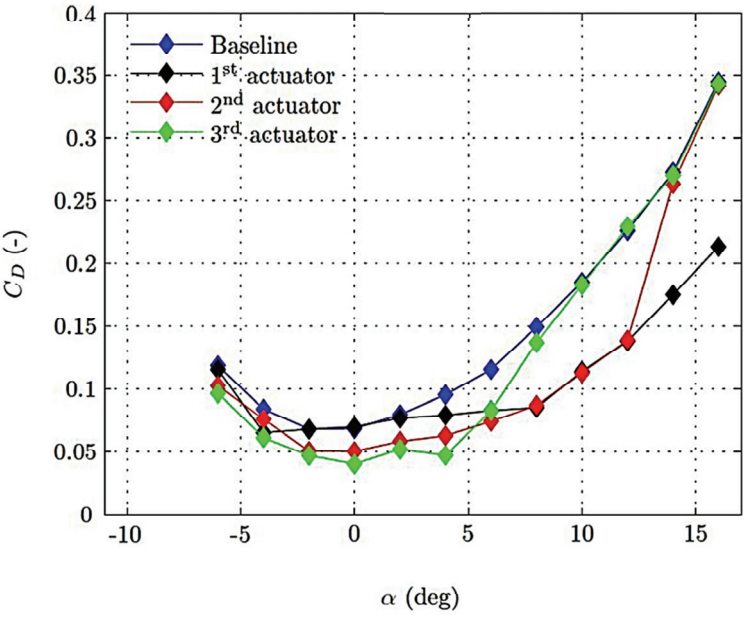
the actuator producing the lowest drag. As α increases, it can be noticed that the best lift and drag coefficients are obtained from actuators located closer to the leading edge in Figs. 1 (a)-(b).

3.2. Particle Image Velocimetry measurements

Flow-field velocity measurements are conducted using a two-velocity-component PIV system in order to further investigate the lift and drag generated by the plasma from actuators at different streamwise locations. In particular we are interested to locate the points of separation above the airfoil by analyzing the PIV measurements. The goal is to study the relation between the actuator location producing the best lift and the lowest drag coefficients established in part 3.1 and its distance to the point of separation. First, we aim to locate the point of separation along the airfoil model without DBD actuation. PIV experiments at Re = 35000 for α ranging from -6° to 16° are conducted. No detached flow is observed for angles below 0°, whereas for positive angles, the flow detaches from the airfoil model. The method of calculation of the point of separation consists in finding the x-location where the streamwise velocity becomes negative at approximately 2.5 mm away from the airfoil model since closer to the model surface PIV reflections prevent finding accurately the position where the streamwise velocity component becomes negative. Once this point is found, a line through it perpendicular to the model surface is drawn to find the location of the point of separation on the airfoil. The evolution of the non-dimensional streamwise position of the point of separation with α is shown in Fig. 2. It can be noticed that the location of the point of separation is closer to the leading edge as α increases. For example, at 16°, the point of separation is located at $x = 0.31c$ while at 0°, the location is $x = 0.87c$. It is interesting to note that the points of separation are located between 30% of the chord and the trailing edge. In the last part of the paper, we are interested to look at the distance between the points of separation discussed above and the position of the actuator to find whether there is a relation between these 2 locations and the lift or drag generated when the actuator is on. Figure 2 indicates that the flow only detaches from 0° onward therefore PIV experiments when the actuators are switched on are carried out only for positive values of α.



(a)



(b)

Fig.1. Variation of the lift coefficient and the drag coefficient with the angle of attack when the 1st, 2nd and 3rd actuators are switched on for *Re* = 35000: (a): C_L; (b): C_D.

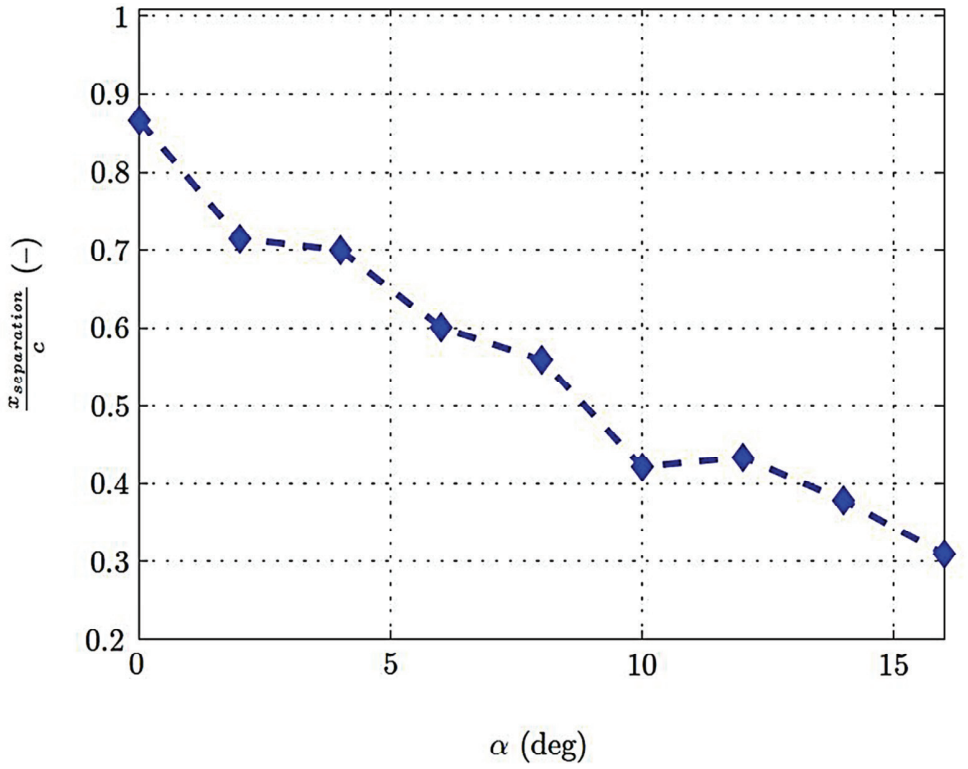


Fig. 2. Variation of the non-dimensional location of the separation point with the angle of attack for *Re* = 35000.

Typical flow field velocity measurements and vorticity contours are shown in Figs. 3 (a)-(d) at α =10° and *Re* = 35000. The flow detaches from the airfoil when none of the actuators is switched on, Fig. 3 (a). When the 1st and 2nd actuators are switched on (green rectangle) respectively in Figs. 3 (b)-(c), the flow is reattached, while the flow is still detached in Fig. 3 (d) when only the 3rd actuator is on (green rectangle). This trend is confirmed in Figs. 1 (a)-(b). From the latter figure, it can be found out that the plasma generated from the 1st and 2nd actuators improves the lift and drag coefficient of the baseline flow at α =10° while the plasma from the 3rd actuator barely improves it. In Figs. 4 (a)-(b), the evolutions of the non-dimensional curvilinear distances between the flow separation points and each of the actuator location with the angles are plotted for *Re* = 35000. In these figures, the black, red and green lines correspond to the distance between the separation point and the 1st, 2nd and 3rd actuators, respectively. Both Figs. 4 (a) and (b) show roughly the same trend. It can be noticed that at each angle, the first actuator in black is located the farthest from the separation point, then comes the second actuator in red and then finally the 3rd actuator in green. For example at 16° in Fig. 4 (a), the first actuator in black is located 0.329*c* ahead of the separation point while the second and third actuators are located at 0.027*c* and 0.359*c* behind the separation point, respectively. In Fig. 4 (a), the actuators producing the best C_L at each angle are connected with a dotted blue line while in Fig. 4 (b), the actuators producing the lowest C_D for each angle are joined with a dotted magenta line. It can be seen that with increasing angles of attack, actuators located closer to the leading edge are more effective. For example, at 0°, the third actuator produces the best lift coefficient in Fig. 4 (a) and the lowest drag coefficient in Fig. 4 (b) while at 6°, the second actuator produces the best C_L and the lowest C_D and finally at 16°, the best actuator is the first one. Figures 4 (a)-(b) clearly indicate that the actuators have to be in front of the separation point to produce the best improvement on the lift and the drag and that no actuators located within the detachment area ($s_{separation} - s_{act} < 0$) produce the best lift or drag. It can also be shown that the effect on the baseline lift and

drag is clearly limited when the actuator is located well within the separation zone. For example in Figs. 1 (a)-(b), the plasma generated from the 2nd actuator has very small effect on the improvement of the baseline lift and drag coefficients at 16°. At that angle, the corresponding actuator is located 0.04*c* behind the separation point shown in Figs. 4 (a)-(b) with a red line. In this section, PIV experiments have been carried out to establish the relation between the position of the actuator and the lift and drag generated when the actuators are switched on. It is observed that the actuators have to be located in front of the separation flow zone to reattach the flow and to improve notably the drag and lift of the airfoil. With increasing angles of attack, actuators need to be located closer to the leading edge to achieve better improvement of the baseline lift and drag coefficients.

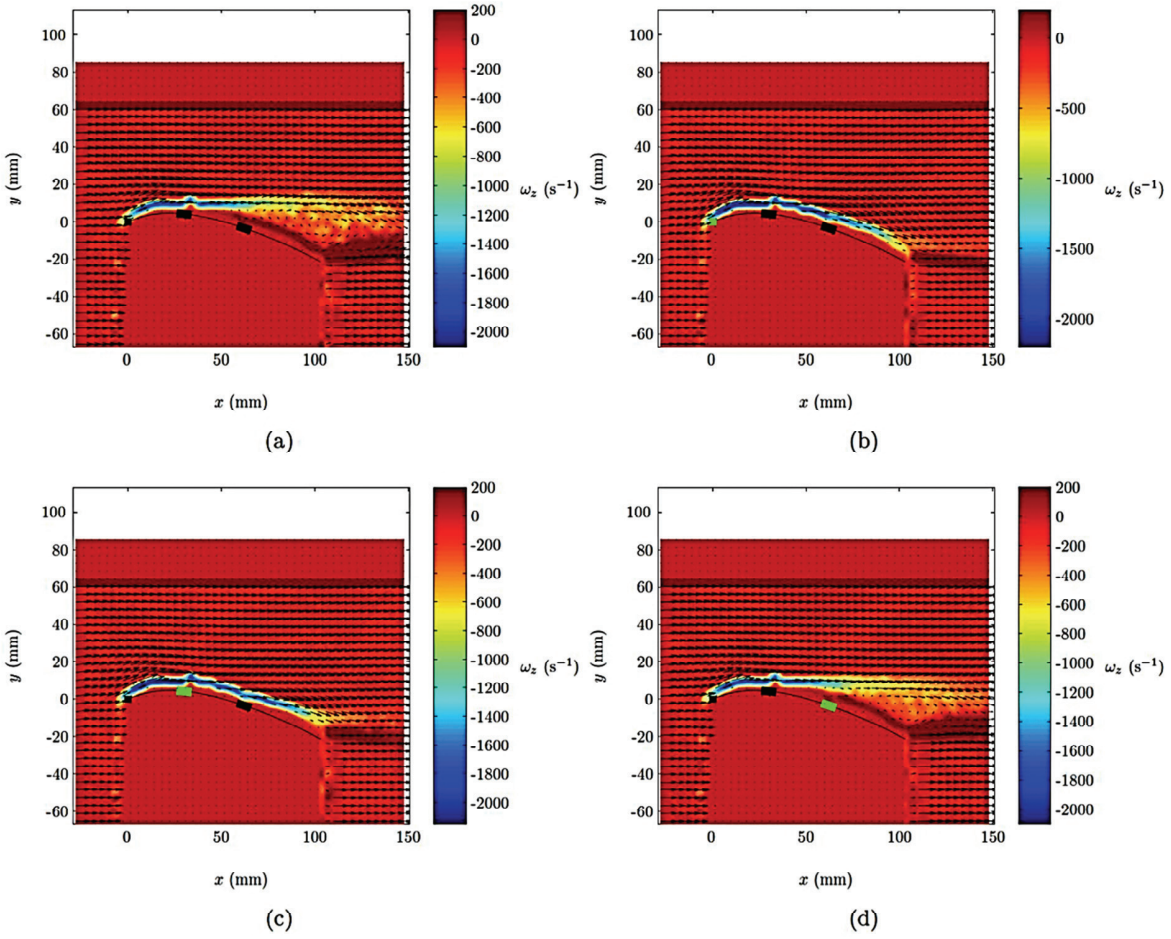
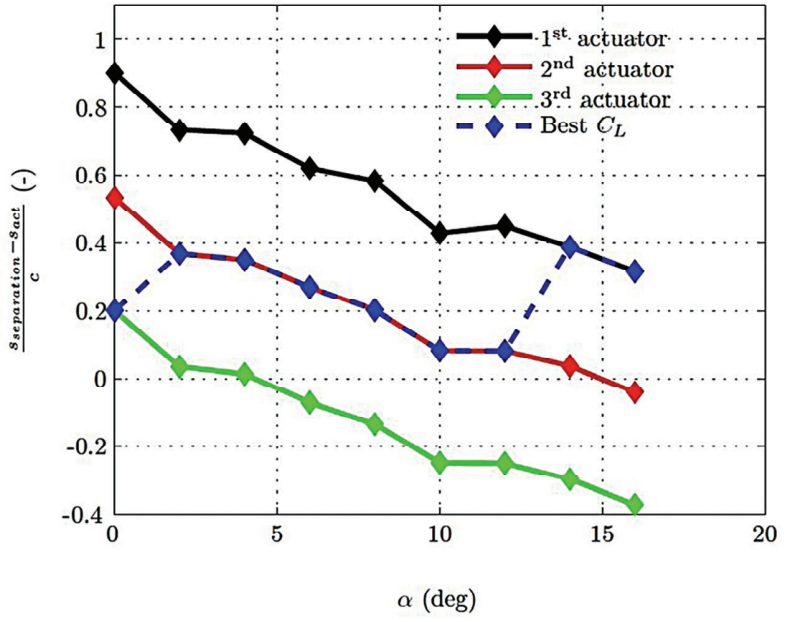
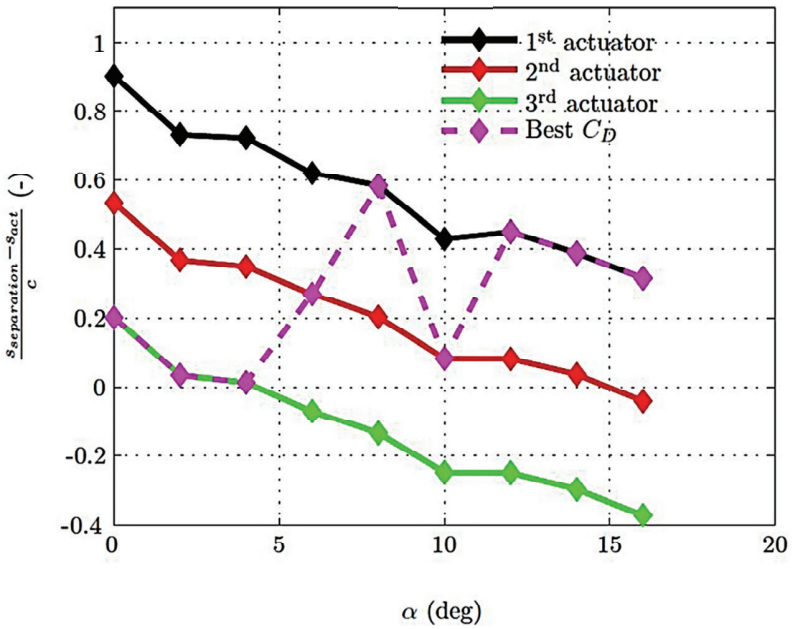


Fig. 3. Velocity vector and vorticity contour plots with the upper surface airfoil curvature and the actuators for an angle of attack of 10° and *Re* = 35000: (a): no actuation; (b): 1st actuator on (green rectangle); (c): 2nd actuator on (green rectangle); (d): 3rd actuator on (green rectangle).



(a)



(b)

Fig. 4 Evolution of the non-dimensional curvilinear distances between the flow separation points and the actuator locations with the angle of attack for $Re = 35000$: (a): actuators associated with the best C_L connected with a dotted blue line; (b): actuators associated with the best C_D joined with a dotted magenta line.

4. Conclusions

In this study, three DBD plasma actuators are mounted on a NACA 4415 airfoil model respectively at the leading edge, 30% and 60% of the chord length. Force balance measurements and Particle Image Velocimetry experiments are conducted at a Reynolds number of 35000 and for angles of attack ranging from -6° to 16°. It is observed that the plasma generated by the actuators can improve the lift and drag of the airfoil by reattaching its flow. For each angle of attack, the location of the separation point on the airfoil surface is identified with its distance from the different actuators calculated. With increasing angles of attack, the best lift and drag are obtained from actuators located closer to the leading edge. It is also shown that the actuator needs to be in front of the separation point to produce the best lift and drag. Actuators located within the separation flow zone have very limited effect on lift and drag.

References

[1] Moreau, E., 2007. Airflow control by non-thermal plasma actuators, Journal of Physics D: Applied Physics 40, pp. 605-636.
[2] Jolibois, J., Forte, M., Moreau, E., 2008. Application of an AC barrier discharge actuator to control airflow separation above a NACA 0015 airfoil: Optimization of the actuation location along the chord, Journal of Electrostatics 66, pp. 496-503.
[3] Little, J., Nishihara, M., Adamovich, I., Samimy, M., 2010. High-lift airfoil trailing edge separation control using a single dielectric barrier discharge plasma actuator, Exp. Fluids 48, pp.521-537.
[4] Zhang, X., Luo, X., Chen, P., 2011. “Airfoil Flow Control Using Plasma Actuation and Coanda Effect”, 29th AIAA Applied Aerodynamics Conference 27 - 30 June 2011, Honolulu, Hawaii, AIAA 2011-3516.



https://dspace.org/

Effects of AC Dielectric Barrier Discharge plasma actuator location on flow separation and airfoil performance

Bouremel, Y.; Li, J. M.; Zhao, Z.; Debiasi, Marco

2014-01-08
Elsevier
https://doi.org/10.1016/j.proeng.2013.12.026
Y. Bouremel, J.M. Li, Z. Zhao, M. Debiasi. Effects of AC Dielectric Barrier Discharge plasma actuator location on flow separation and airfoil performance. Procedia Engineering, Volume 67, 2013, Pages 270-278

Downloaded from a DSpace repository. https://dspace.org/